nature astronomy

ARTICLES

https://doi.org/10.1038/s41550-018-0538-5

Discovery of a proton aurora at Mars

J. Deighan[1]*, S. K. Jain[1], M. S. Chaffin[1], X. Fang[1], J. S. Halekas[2], J. T. Clarke[3], N. M. Schneider[1], A. I. F. Stewart[1], J.-Y. Chaufray[4], J. S. Evans[5], M. H. Stevens[6], M. Mayyasi[3], A. Stiepen[7], M. Crismani[1], W. E. McClintock[1], G. M. Holsclaw[1], D. Y. Lo[8], F. Montmessin[4], F. Lefèvre[4] and B. M. Jakosky[1]

Proton aurorae are a distinct class of auroral phenomena caused by energetic protons precipitating into a planetary atmosphere. The defining observational signature is atomic hydrogen emissions from the precipitating particles after they obtain an electron from the neutral atmospheric gas, a process known as charge exchange. Until now, proton aurorae have been observed at Earth only. Here, we present evidence of auroral activity driven by precipitating protons at Mars, using observations by the MAVEN spacecraft. We observed transient brightening of upper atmospheric hydrogen Lyman-α emission across the Martian dayside correlated with solar wind activity. The driving mechanism is one not found at Earth and originates from energetic neutral atom production by solar wind protons directly interacting with the extended hydrogen corona surrounding Mars. We characterize this new type of Martian aurora and compare the observed emissions with preliminary modelling guided by simultaneous in situ particle measurements. These observations provide insights into how the solar wind can directly deposit energy into the Martian atmosphere as well as all other planetary objects that are surrounded by a substantial neutral corona exposed to the solar wind.

Proton aurorae were first recognized at Earth by the presence of Balmer Hα and Hβ visible spectral lines associated with other more typical auroral emissions from the atmosphere[1]. These photons are emitted by excited hydrogen atoms produced from charge exchange reactions, and the precipitating particles may repeatedly transition from protons to energetic neutral atoms (ENAs) and back again. These differ from more typical auroral emissions because they originate from the precipitating energetic particles themselves rather than excited atmospheric atoms and molecules[2]. As a result, the hydrogen emission lines are Doppler shifted, providing an additional observational signature regularly used to identify and study proton aurorae at Earth[3].

The characteristics of proton aurorae at Earth are dominated by the strong intrinsic magnetic field, which deflects the solar wind and controls where plasma can interact with the upper atmosphere[4]. The situation is different for planets without such a strong global magnetic field. Kallio and Barabash[5] hypothesized an extraterrestrial mechanism for proton aurorae at Mars, which both lacks a global magnetic field and is surrounded by an extensive corona of neutral hydrogen (see Fig. 1). In this process, solar wind protons upstream of the bow shock charge exchange with the coronal neutral hydrogen to produce ENAs retaining the solar wind direction and kinetic energy (~1 keV). The ENAs continue freely through the bow shock to deposit their energy in the lower thermosphere at altitudes of 110–130 km, producing ionization, dissociation, heating, excitation and auroral emissions. With only slight aberrations from the apparent direction of the Sun, these ENAs shower down on the dayside of the planet similarly to solar photons, resulting in reduced energy flux at higher solar zenith angles (SZAs) and with no direct access to the nightside of the planet. Partially thermalized plasma from the magnetosheath may also produce a more diffuse population of precipitating ENAs with limited access to the night hemisphere.

Specific types of aurora at Earth bear some resemblance to this extraterrestrial phenomenon. The IMAGE (Imager for Magnetopause-to-Aurora Global Exploration) mission has observed proton aurorae in the cusp region caused by direct access of magnetosheath plasma[6], but this depends on a specific magnetic configuration and does not involve conversion of protons to ENAs to bypass the magnetic field as a key step. Conversion of energetic ions to ENAs does occur in the ring current at Earth and is thought to drive low and mid-latitude dayside aurorae observed by the STP 78-1 satellite[7], but the ions in this case are not directly derived from the solar wind. Thus, Martian proton aurorae offer valuable insights into direct interactions of the solar wind with a planet's upper atmosphere in a way that does not occur at Earth. In principle, this mechanism can occur at any planetary body that is surrounded by a neutral hydrogen corona and that lacks a strong global magnetic field. Mars provides a natural and convenient laboratory for understanding this class of star–planet interactions.

Observations

In this study, we used the data from two instruments on board the MAVEN (Mars Atmosphere and Volatile EvolutioN) mission, which is dedicated to understanding the variability of the upper atmosphere of Mars and its interactions with solar radiation and solar wind inputs[8]. The MAVEN orbit has a period of 4.5 h and an elliptical shape, which allows it to sample within the thermosphere and ionosphere at periapsis (150 km) and exterior to the bow shock at apoapsis (6,200 km). We examined periapse data from the time period of 2015 March 01 to 2015 April 04 (MAVEN orbits 812–986), during the declining phase of solar cycle 24.

The Imaging Ultraviolet Spectrograph (IUVS) instrument measures numerous airglow emissions using separate far-UV (110–190 nm) and mid-UV (180–340 nm) channels[9]. Near periapsis, it acquires up to 12 limb scans of the thermosphere at different

[1]Laboratory for Atmospheric and Space Physics, University of Colorado at Boulder, Boulder, CO, USA. [2]Department of Physics and Astronomy, University of Iowa, Iowa City, IA, USA. [3]Center for Space Physics, Boston University, Boston, MA, USA. [4]LATMOS/IPSL, Guyancourt, France. [5]Computational Physics, Inc, Springfield, VA, USA. [6]Space Science Division, Naval Research Laboratory, Washington, DC, USA. [7]LPAP, STAR, University of Liège, Liege, Belgium. [8]LPL, University of Arizona, Tucson, AZ, USA. *e-mail: Justin.Deighan@lasp.colorado.edu

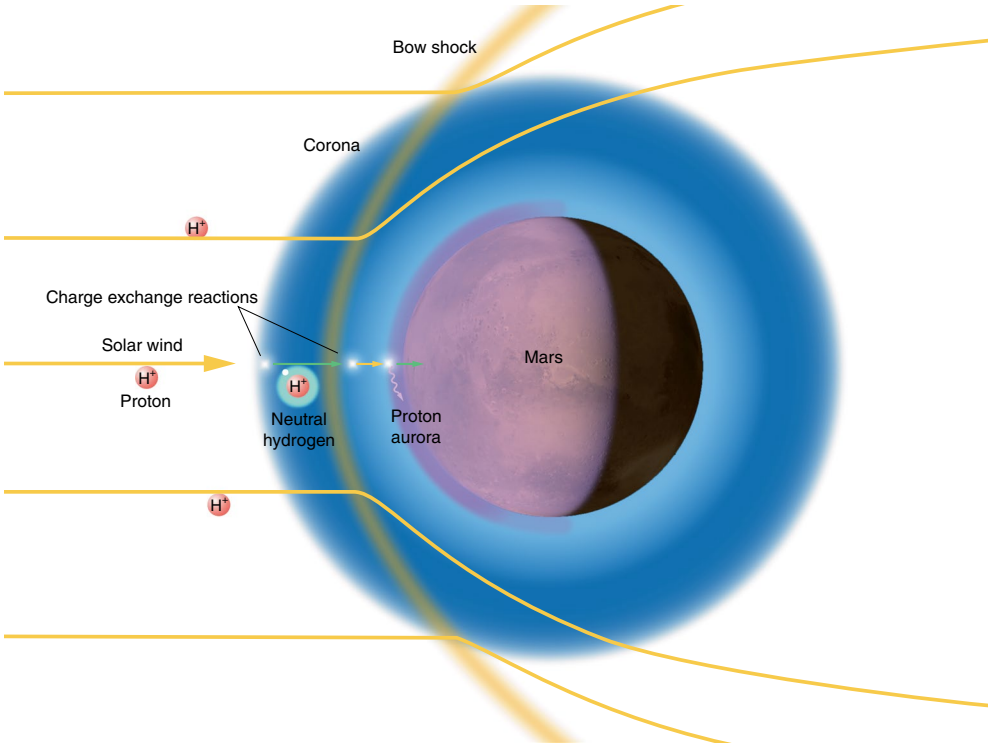

Fig. 1 | Mechanism for Martian proton aurorae originating from solar wind charge exchange. Upstream solar wind protons (H^+) are typically deflected by the Martian bow shock (yellow stream lines), but some charge exchange with neutral hydrogen in the corona (blue), becoming energetic neutral particles (shown as a proton surrounded by a shell (cyan) containing an electron (white dot)). These neutral particles freely pass through the bow shock while retaining the original kinetic energy and direction of the solar wind (green arrow) and deposit energy in the planet's thermosphere. A fraction of this energy is emitted from the energetic hydrogen as Doppler-shifted Lyα photons.

locations around the planet by looking across-track of the spacecraft motion. There are occasional gaps in the data due to sharing pointing priority with other instruments and communication passes. In this study, we examined the IUVS dayside limb scans to look for anomalous thermospheric features in the vertical brightness profile of hydrogen Lyman α (Lyα) at 121.6 nm. Under typical conditions, Lyα is dominated by optically thick resonant fluorescent scattering in the Martian dayglow[10–12].

However, the mere detection of a Lyα anomaly in an IUVS airglow limb scan does not necessarily indicate the specific process for its origin. To confirm an interpretation of proton aurorae, a simultaneous indication of the energetic particle environment must be included. We therefore examined data from the Solar Wind Ion Analyzer (SWIA) on board MAVEN, which is designed to measure ions with energies of 5 eV to 25 keV both in the upstream solar wind and within the Martian magnetosphere[13]. It was previously reported that the SWIA detected a time-variable population of nearly monoenergetic protons with velocity essentially unchanged from that of the solar wind in the dayside thermosphere appearing below 250 km during the selected time frame[14]. These protons were identified as being the product of charge exchange by penetrating ENAs[5], and it was speculated that there might be associated UV proton aurorae. During this time frame, the Martian southern hemisphere was in summer (solar longitude ~300°), and the global hydrogen corona was seasonally inflated, enhancing charge exchange with the solar wind[15].

Note that the volume of atmospheric emission observed by the IUVS is not directly co-located with the in situ measurement made by the SWIA. For example, the tangent point of an IUVS limb scan taken at an altitude of 400 km will be separated from the spacecraft location by 1,400 km, or approximately 24° geographically. However, the Martian proton aurorae produced by upstream solar-wind-sourced ENAs should elicit a global response in the dayside thermosphere and register in the data of both instruments.

Results

Two sets of airglow data from adjacent orbits in Fig. 2 demonstrate the observed atomic hydrogen emission signature of a Martian proton aurora. Several prominent UV dayglow features associated with carbon dioxide (CO_2) ionization and dissociation products are included for context[16–18]. The data for orbit 985 are typical of the Martian UV dayglow: all features exhibit a strong peak at 130 km, except for Lyα, which presents a relatively flat profile due to multiple scattering and the large scale height of atomic hydrogen. In contrast, data acquired 4.5 h later on orbit 986 show that the Lyα profile has developed a strongly peaked brightening. The enhancement is diffuse, being evident in all limb scans and along the entire 10.6° length of the IUVS slit. There is also a pronounced SZA dependence, with the brightest peaks having SZAs of less than 40°, and the signal diminishing into the background as the terminator is approached. In the first few scans, the enhancement exceeds 4,000 rayleigh units (R) of photon flux, a 40% increase over the background fluorescent source, which is a highly significant change given that Lyα has a signal-to-noise ratio of more than 100 at this altitude. The brightnesses of the emission features from CO_2 products are not significantly changed between the two orbits. Examination of the SWIA data indicates a threefold increase in the flux of penetrating protons in the thermosphere from orbit 985 to orbit 986, from $2.6\times10^5\,cm^{-2}\,s^{-1}$ to $7.8\times10^5\,cm^{-2}\,s^{-1}$.

The regular coverage of IUVS and SWIA data enables us to construct an orbit-by-orbit timeline of thermospheric Lyα brightening and penetrating proton flux (Fig. 3). This shows that events with

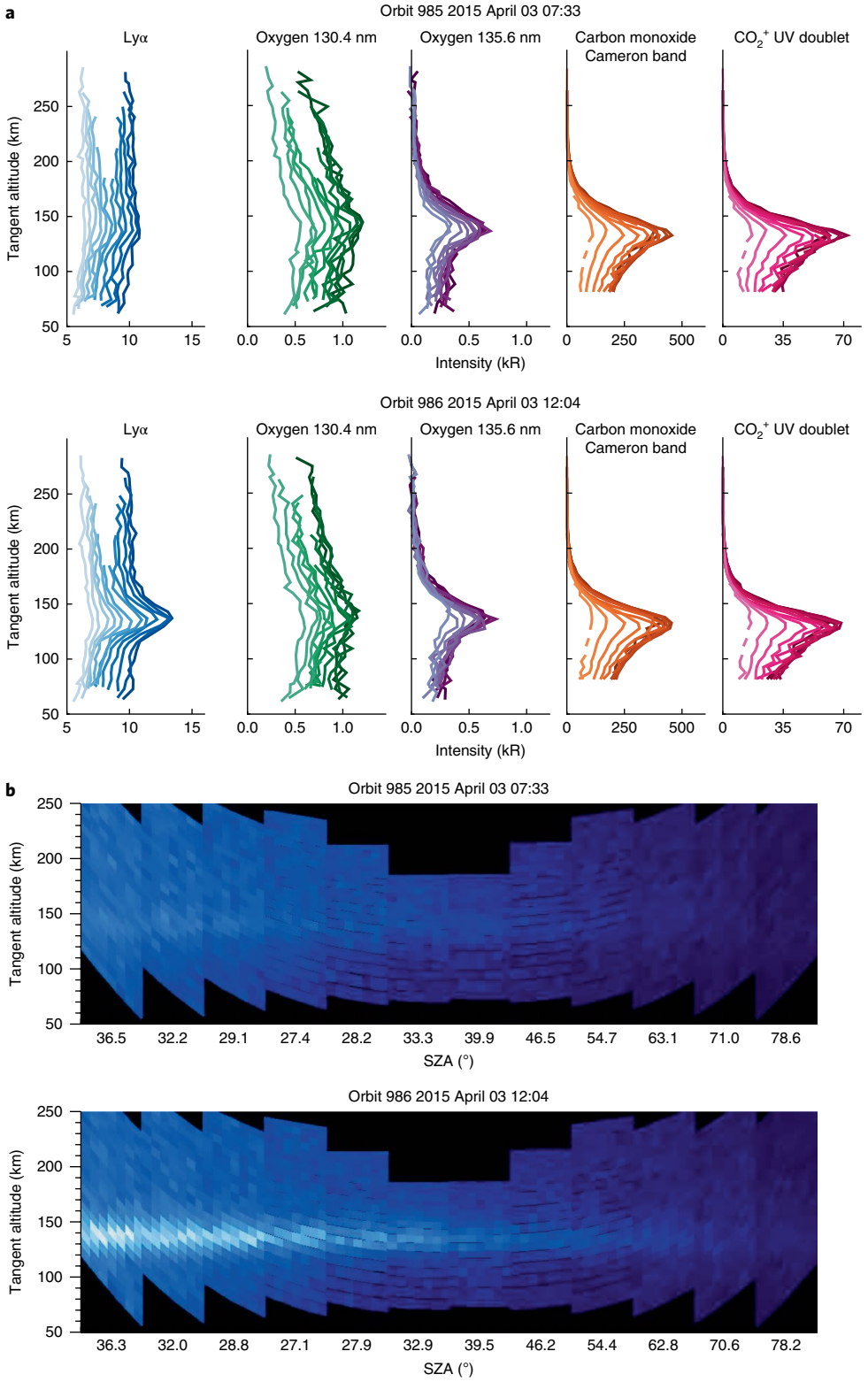

Fig. 2 | Limb observations showing the signature of a proton aurora in atomic hydrogen emission. a, IUVS-observed brightness profiles for Lyα and several CO_2 ionization and dissociation products on MAVEN orbits 985 and 986. Each emission plot contains profiles from 12 limb scans, with shading from dark to light indicating chronological order of acquisition. Additional geometry is in Supplementary Fig. 1. **b**, The same Lyα brightnesses in a synthetic image format, showing the illumination of 12 limb scans ordered from left to right. Each scan has 21 integrations (vertical) with 7 spatial samples along the length of the 10.6° IUVS airglow slit (horizontal). For both orbits, CO_2 absorption of Lyα becomes important for tangent altitudes of less than 120 km.

strongly brightened Lyα peaks are not very common, occurring on just a few of the orbits. During the orbits where both instruments acquired data, there is a clear correlation between the presence of a Lyα peak and an enhancement in the penetrating proton flux. These events persist for at most a few orbits, indicating time variability of the order of hours or less. The proton flux is derived from SWIA

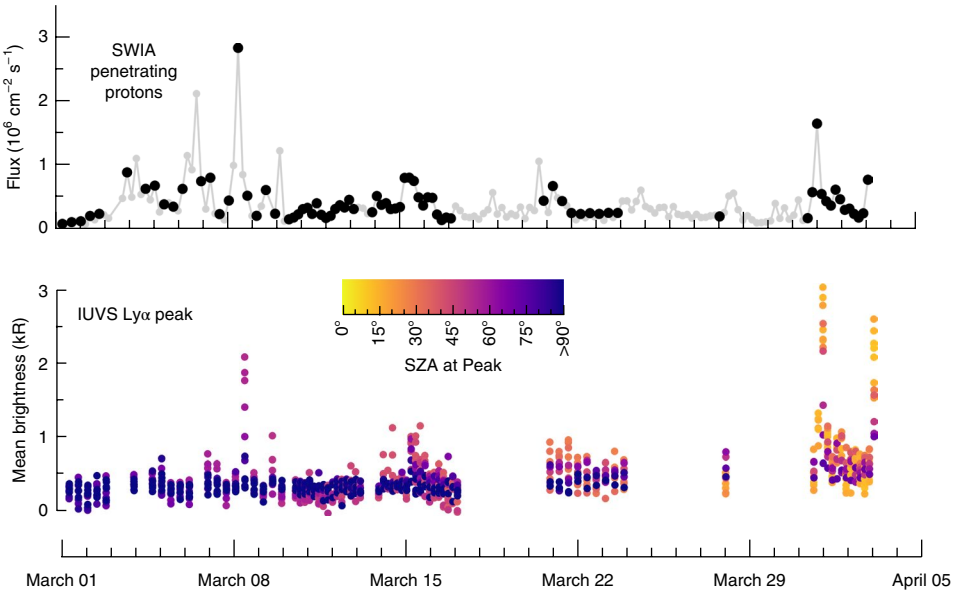

Fig. 3 | Timeline of SWIA penetrating protons and IUVS Lyα enhancements in March–April 2015. SWIA fluxes are single-valued per orbit, based on the dayside portion of periapse data. SWIA data points have a larger, black symbol when a joint IUVS observation set is available. IUVS data contain values for each of the 12 limb scans per orbit, representing the mean brightness from 110 km to 160 km where peaks occur. Each sample is coloured according to the SZA of the tangent point at the peak. An estimate of the background fluorescent Lyα source has been subtracted using the mode of the brightness above 160 km. The event shown in Fig. 2 is the rightmost sample in the timeline.

data taken on the dayside portion of the orbit where the penetrating population is observed, while IUVS limb scans at all SZAs are included. The trend of greater brightening at lower SZAs is a consistent feature among all the events, and there are no observations during this time showing strong brightening at SZAs of more than 90°. Note that the range of SZAs sampled on each orbit varies through this time period due to precession of the MAVEN orbit.

Preliminary modelling was performed to assess whether the characteristics of the observed Lyα emission enhancements support the interpretation of a proton aurora. We adapted a Monte Carlo ion transport model that has been applied for Earth proton aurora studies[19,20], carefully accounting for the finite gyroradius effects within the weak Martian magnetic field environment. Sensitivity analysis indicated that although local magnetic field configuration could perturb the flux of precipitating protons, it does not substantially impact the altitude of peak energy deposition or the interpretation of the data presented here. Energy-dependent hydrogen and proton cross-sections and collisional scattering properties appropriate for the Martian thermosphere were adopted[5,21]. The SWIA measurements were used to guide precipitation of monoenergetic hydrogen ENAs at the top of an a priori model thermosphere, with data reduction as described in a previous study[14]. The model CO_2 altitude profile was confirmed to be consistent with the CO_2 density profiles retrieved over 130–193 km from IUVS airglow measurements made during this time period[22], as shown in Supplementary Fig. 3. Further details are provided in Methods.

The most extreme events in this time period were found on MAVEN orbits 850 (2015 March 08), 975 (2015 April 01) and 986 (2015 April 03). These three orbits each have at least one limb scan sampled at SZAs of 62°–66°, making a consistent comparison of characteristics possible. Model results for these orbits qualitatively support the interpretation of the peaked Lyα enhancements discovered by the IUVS as being a proton aurora produced by ENAs associated with the penetrating protons observed by the SWIA (Fig. 4). The observed vertical shape of the profile is well reproduced by the model for all cases. The relative peak brightnesses are reasonably well predicted, although orbit 975 is overestimated. A notable discrepancy is that the altitudes of the model-predicted peaks are systematically lower than those observed, by approximately 7 km. This may be due to uncertainties in the cross-sections for the CO_2 interactions, some of which are estimated from other species. Using the model prediction of secondary electrons for orbit 986, we estimate that the maximum auroral emission from CO_2 ionization and dissociation is less than 1% compared with the normal dayglow. This is consistent with the lack of discernible response observed by the IUVS in UV airglow features other than Lyα.

Discussion and implications

All previously reported observations of auroral activity at Mars have been on the nightside and identified as being due to electron precipitation. Because the orbit of Mars is external to that of Earth, its nightside cannot be well observed from Earth, and all auroral detections have been made by spacecraft at Mars. The Mars Express SPICAM (SPectroscopy for Investigation of Characteristics of the Atmosphere of Mars) instrument made the first detection of discrete electron aurorae by observing UV emissions geographically associated with strong crustal magnetic fields[23]. More recently, global diffuse electron aurorae associated with solar energetic particle events were discovered by the MAVEN IUVS[24]. The UV spectrum of an electron aurora is similar to that of the dayglow produced by solar extreme UV radiation, because both originate primarily from CO_2 ionization and dissociation products. These previous identifications of aurorae depended on the observations being on the nightside, where UV dayglow did not complicate analyses.

We find that the Martian proton aurorae observed by the IUVS are located primarily on the dayside of the planet, with peak emission at altitudes comparable to that of the UV dayglow peak. This dayglow obscures the auroral emissions from CO_2 products, so we must rely on the atomic hydrogen emission for definitive identification and characterization of proton aurorae. Due to the large vertical scale height of atomic hydrogen (more than 500 km), and Lyα photons from thermal hydrogen being multiply scattered in the Martian thermosphere, observed vertical brightness profiles of this emission are typically flat and featureless. The auroral emission vertical scale

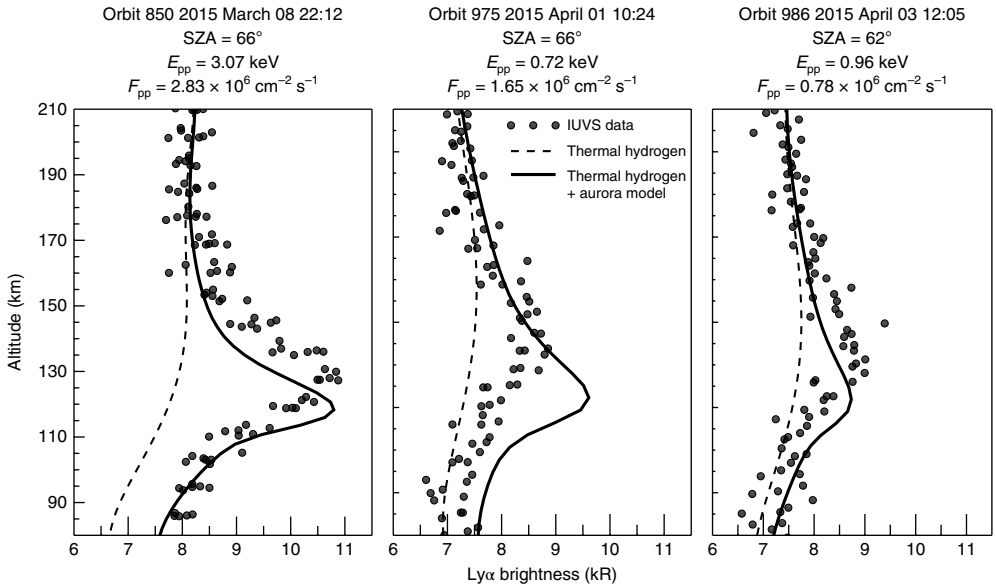

Fig. 4 | Observed and modelled Lyα brightness profiles. Symbols indicate limb observations made by the IUVS, dashed lines are estimated fluorescent scattering by thermal hydrogen using nearby orbits that lack a peak and solid lines are aurora model output guided by SWIA-measured penetrating proton characteristics. The SZA of the limb scan as well as the energy (E_{pp}) and flux (F_{pp}) of penetrating protons are recorded at the top of each plot. Details of the modelling are discussed in the text.

height is more similar to the density profile of collision partners, which in this case is approximately 12 km for the CO_2-dominated lower thermosphere. Doppler-shifted hydrogen emissions from proton aurorae avoid absorption by the ambient neutral hydrogen and appear vertically peaked and optically thin, resulting in substantial limb brightening. However, even the most extreme events discussed here would manifest as an increase of less than 5% in the brightness of Lyα for a nadir-viewing observation of the planet.

Although the preliminary modelling presented here supports the interpretation of a proton aurora, more detailed work is warranted. The treatment of the precipitating particles as a monoenergetic beam and the use of a penetrating proton flux derived from SWIA data averaged over the periapsis pass are oversimplifications. Previous detailed modelling of the Martian magnetosphere has shown that during enhanced solar wind conditions, there should be a substantial flux of precipitating ENAs produced from thermalized plasma in the magnetosheath[25,26], and this has been confirmed in observations made by Mars Express and MAVEN[15,27]. In addition, there is evidence in the IUVS data for variability of the Lyα peak brightness that is uncorrelated with the SZA, as seen in Fig. 2 for the first seven limb scans with SZAs of less than 40°. This may be due to time variability of the precipitating particle population over the course of the 12 min it took the IUVS to acquire the limb scans. This short-term variability could explain why we do not exactly reproduce the relative peak brightnesses of the scans when scaling using the time-averaged SWIA data. To go beyond the relative comparison of a few events performed in this study would require a three-dimensional global model to properly synthesize the SWIA and IUVS data, due to the inherent separation between the in situ and remote-sensing observations.

The processes that produce the Martian proton aurora reported here should occur at any planetary body with a substantial neutral corona that extends beyond its bow shock and that can directly interact with the solar wind. These conditions are known to occur at Venus[28] and comets[29] and should also be present at the moon Titan when it is outside Saturn's magnetosphere[30]. We can speculate that such proton aurorae may also exist at exoplanets such as HD 209458 b, which orbits very close to its parent star and has been found to be surrounded by a highly extended neutral hydrogen envelope[31]. This mechanism for generating proton aurorae is distinct from any of the processes found at Earth, and the data being collected by MAVEN provide an opportunity to observationally study a truly extraterrestrial type of aurora.

Methods

Aurora modelling. For candidate proton aurora events, the precipitating ENA population was assumed to be monoenergetic, with the same energy as the undispersed core of the SWIA-measured penetrating proton population on the same orbit. The ENA flux input to the model was specified to reproduce the measured penetrating proton flux in the altitude range of 150–250 km. Vertical profiles of these model fluxes are shown in Supplementary Fig. 3. The resulting volume emission rates for Lyα, as shown in Supplementary Fig. 4, were then integrated along the IUVS line of sight to produce a brightness profile. For the events examined, we calculate from the observed penetrating proton velocity and line-of-sight phase angles that the auroral Lyα photons would be redshifted by 130–630 km s^{-1}. This amounts to a wavelength shift of 0.005–0.026 nm, which is well below the 0.7 nm spectral resolution of the IUVS for this data set. This Doppler shift is large enough that we may neglect scattering by ambient thermal hydrogen. However, absorption by CO_2 was found to be non-negligible near and below the altitude of the peak. For comparison with the data, we applied a scale factor to the auroral model brightness profiles, which was chosen to match the peak intensity of the event examined on orbit 850.

Fluorescent Lyα background. To compare the auroral model output with the IUVS Lyα observations requires an estimate of the fluorescent thermal hydrogen background, which is approximately 7–8 kR at the altitude of the auroral emission. This source is difficult to model due to it being optically thick, but when a bright peak is absent, the brightness profile is typically repeatable (within ~5%) for each of the 12 limb scans when adjacent orbits are compared, that is, the first limb scan of one orbit is very similar to the first scan of the next orbit. We took advantage of this and estimated the fluorescent source during the peak brightening events by using profiles acquired on nearby orbits with low penetrating proton flux and no apparent peak brightening. First, a fifth-order polynomial fit was made to the vertical brightness profile from an orbit without aurorae. This was then used to estimate the background on an orbit with aurorae by scaling the polynomial function such that the mode of the brightness matched at altitudes > 170 km. At these altitudes, the fluorescent source greatly dominates over any auroral emission. The scale factor was within 6% of unity for the three events reported here.

Data availability. The MAVEN IUVS data used in this study are publicly archived with the Planetary Atmospheres node of the Planetary Data System and are identified by filenames with the orbit number, the label 'periapse' and 'v07' as

the version. The MAVEN SWIA data are publicly archived with the Planetary Plasma Interactions node of the Planetary Data System. The data that support the plots within this paper and other findings of this study are available from the corresponding author upon reasonable request.

Received: 13 December 2017; Accepted: 26 June 2018;
Published online: 23 July 2018

References

1. Vegard, L. Hydrogen showers in the auroral region. *Nature* **144**, 1089–1090 (1939).
2. Eather, R. H. Auroral proton precipitation and hydrogen emissions. *Rev. Geophys.* **5**, 207–285 (1967).
3. Gérard, J.-C., Hubert, B., Bisikalo, D. V. & Shematovich, V. I. A model of the Lyman line profile in the proton aurora. *J. Geophys. Res.* **105**, 15795–15806 (2000).
4. Hardy, D. A., Gussenhoven, M. S. & Brautigam, D. A statistical model of auroral ion precipitation. *J. Geophys. Res.* **94**, 370–392 (1989).
5. Kallio, E. & Barabash, S. Atmospheric effects of precipitating energetic hydrogen atoms on the Martian atmosphere. *J. Geophys. Res.* **106**, 165–177 (2001).
6. Frey, H. U. et al. Proton aurora in the cusp. *J. Geophys. Res.* **107**, 1091 (2002).
7. Stephan, A. W., Chakrabarti, S. & Cotton, D. M. Evidence of ENA precipitation in the EUV dayglow. *Geophys. Res. Lett.* **27**, 2865–2868 (2000).
8. Jakosky, B. M. et al. The Mars Atmosphere and Volatile Evolution (MAVEN) mission. *Space Sci. Rev.* **195**, 3–48 (2015).
9. McClintock, W. E. et al. The Imaging Ultraviolet Spectrograph (IUVS) for the MAVEN mission. *Space Sci. Rev.* **195**, 75–124 (2015).
10. Anderson, D. E.Jr & Hord, C. W. Mariner 6 and 7 ultraviolet spectrometer experiment: analysis of hydrogen Lyman-alpha data. *J. Geophys. Res.* **76**, 6666–6673 (1971).
11. Chaufray, J. Y., Bertaux, J. L., Leblanc, F. & Quémerais, E. Observation of the hydrogen corona with SPICAM on Mars Express. *Icarus* **195**, 598–613 (2008).
12. Chaffin, M. S. et al. Three-dimensional structure in the Mars H corona revealed by IUVS on MAVEN. *Geophys. Res. Lett.* **42**, 9001–9008 (2015).
13. Halekas, J. S. et al. The Solar Wind Ion Analyzer for MAVEN. *Space Sci. Rev.* **195**, 125–151 (2015).
14. Halekas, J. S. et al. MAVEN observations of solar wind hydrogen deposition in the atmosphere of Mars. *Geophys. Res. Lett.* **42**, 8901–8909 (2015).
15. Halekas, J. S. Seasonal variability of the hydrogen exosphere of Mars. *J. Geophys. Res.* **122**, 901–911 (2017).
16. Barth, C. A. et al. Mariner 6 and 7 ultraviolet spectrometer experiment: upper atmosphere data. *J. Geophys. Res.* **76**, 2213–2227 (1971).
17. Leblanc, F., Chaufray, J. Y., Lilensten, J., Witasse, O. & Bertaux, J.-L. Martian dayglow as seen by the SPICAM UV spectrograph on Mars Express. *J. Geophys. Res.* **111**, E09S11 (2006).
18. Jain, S. K. et al. The structure and variability of Mars upper atmosphere as seen in MAVEN/IUVS dayglow observations. *Geophys. Res. Lett.* **42**, 9023–9030 (2015).
19. Fang, X., Liemohn, M. W., Kozyra, J. U. & Solomon, S. C. Quantification of the spreading effect of auroral proton precipitation. *J. Geophys. Res.* **109**, A04309 (2004).
20. Fang, X., Lummerzheim, D. & Jackman, C. H. Proton impact ionization and a fast calculation method. *J. Geophys. Res.* **118**, 5369–5378 (2013).
21. Basu, B., Jasperse, J. R., Robinson, R. M., Vondrak, R. R. & Evans, D. S. Linear transport theory of auroral proton precipitation—a comparison with observations. *J. Geophys. Res.* **92**, 5920–5932 (1987).
22. Evans, J. S. et al. Retrieval of CO_2 and N_2 in the Martian thermosphere using dayglow observations by IUVS on MAVEN. *Geophys. Res. Lett.* **42**, 9040–9049 (2015).
23. Bertaux, J.-L. et al. Discovery of an aurora on Mars. *Nature* **435**, 790–794 (2005).
24. Schneider, N. M. et al. Discovery of diffuse aurora on Mars. *Science* **350**, aad0313 (2015).
25. Kallio, E. S., Luhmann, J. G. & Barabash, S. Charge exchange near Mars: the solar wind absorption and energetic neutral atom production. *J. Geophys. Res.* **102**, 22183–22197 (1997).
26. Diéval, C., Kallio, E., Stenberg, G., Barabash, S. & Jarvinen, R. Hybrid simulations of proton precipitation patterns onto the upper atmosphere of Mars. *Earth Planets Space* **64**, 121–134 (2012).
27. Gunell, H. et al. First ENA observations at Mars: charge exchange ENAs produced in the magnetosheath. *Icarus* **182**, 431–438 (2006).
28. Gombosi, T. I., Cravens, T. E., Nagy, A. F., Elphic, R. C. & Russell, C. T. Solar wind absorption by Venus. *J. Geophys. Res.* **85**, 7747–7753 (1980).
29. Simon Wedlund, C. et al. The atmosphere of comet 67P/Churyumov-Gerasimenko diagnosed by charge-exchanged solar wind alpha particles. *Astron. Astrophys.* **587**, A154 (2016).
30. Bertucci, C. et al. Titan's interaction with the supersonic solar wind. *Geophys. Res. Lett.* **42**, 193–200 (2015).
31. Vidal-Madjar, A. et al. An extended upper atmosphere around the extrasolar planet HD209458b. *Nature* **422**, 143–146 (2003).

Acknowledgements

The MAVEN mission is supported by NASA through the Mars Exploration Program. J.-Y.C., F.M. and F.L. are funded by the programme 'Systeme Solaire' of Centre National d'Etudes Spatiales. A.S. is supported by the Belgian Fund for Scientific Research (FNRS).

Author contributions

J.D., S.K.J. and M.S.C. performed the analysis. X.F. created and ran the precipitating particle transport model used here. J.S.H. provided SWIA measurements and guidance in using them. J.S.E. provided neutral atmosphere airglow retrievals. All authors contributed to the development of the instrument pipeline and/or data acquisition as well as interpretation and presentation of these results.

Competing interests

The authors declare no competing interests.

Additional information

Supplementary information is available for this paper at https://doi.org/10.1038/s41550-018-0538-5.

Reprints and permissions information is available at www.nature.com/reprints.

Correspondence and requests for materials should be addressed to J.D.

Publisher's note: Springer Nature remains neutral with regard to jurisdictional claims in published maps and institutional affiliations.